366 J. Med. Chem. 2011, 54, 366–373
DOI: 10.1021/jm101230g

Journal of Medicinal Chemistry Article

# Evaluation of Novel $N^1$-Methyl-2-phenylindol-3-ylglyoxylamides as a New Chemotype of 18 kDa Translocator Protein-Selective Ligand Suitable for the Development of Positron Emission Tomography Radioligands

Victor W. Pike,*[,†] Sabrina Taliani,[‡] Talakad G. Lohith,[†] David R. J. Owen,[§] Isabella Pugliesi,[‡] Eleonora Da Pozzo,[∥] Jinsoo Hong,[†] Sami S. Zoghbi,[†] Roger N. Gunn,[⊥] Christine A. Parker,[⊥] Eugenii A. Rabiner,[§,⊥] Masahiro Fujita,[†] Robert B. Innis,[†] Claudia Martini,[∥] and Federico Da Settimo*[,‡]

[†]*Molecular Imaging Branch, National Institute of Mental Health, National Institutes of Health, Building 10, Room B3 C346A, 10 Center Drive, Bethesda, Maryland 20892, United States,* [‡]*Dipartimento di Scienze Farmaceutiche, Università di Pisa, Via Bonanno 6, 56126 Pisa, Italy,* [§]*Department of Experimental Medicine and Toxicology, Imperial College London, Hammersmith Hospital, London, United Kingdom,* [∥]*Dipartimento di Psichiatria, Neurobiologia, Farmacologia e Biotecnologie, Università di Pisa, Via Bonanno 6, 56126 Pisa, Italy, and* [⊥]*Clinical Imaging Centre, GlaxoSmithKline, London, United Kingdom*

*Received September 22, 2010*

A novel series of $N^1$-methyl-(2-phenylindol-3-yl)glyoxylamides, **19**−**31**, designed in accordance with our previously reported pharmacophore/topological model, showed high affinity for the 18 kDa translocator protein (TSPO) and paved the way for developing a new radiolabeled probe. Thus ligand **31**, *N*,*N*-di-*n*-propyl-($N^1$-methyl-2-(4′-nitrophenyl)indol-3-yl)glyoxylamide, featuring the best combination of affinity and lipophilicity, was labeled with carbon-11 for evaluation with positron emission tomography (PET) in monkey. After intravenous injection, [$^{11}$C]**31** entered brain to give a high proportion of TSPO-specific binding. These findings augur well for the future application of [$^{11}$C]**31** in humans. Consequently, the binding of **31** to human TSPO was tested on samples of brain membranes from deceased subjects who through ethically approved in vitro study had previously been established to be high-affinity binders (HABs), mixed-affinity binders (MABs), or low-affinity binders (LABs) for the known TSPO ligand, PBR28 (**2**). **31** showed high affinity for HABs, MABs, and LABs. In conclusion, [$^{11}$C]**31** represents a promising new chemotype for developing novel TSPO radioligands as biomarkers of neuroinflammation.

## Introduction

Translocator protein (TSPO[a]), formerly known as the peripheral benzodiazepine receptor or PBR, is an 18 kDa protein which is mainly located at the contact sites between the outer and inner mitochondrial membranes. This receptor is a component of a trimeric complex with the 32 kDa voltage-dependent anion channel (VDAC) and the 30 kDa adenine nucleotide translocase (ANT) to constitute the mitochondrial permeability transition pore (MPTP).[1,2]

TSPO is involved in a variety of biological processes, such as cholesterol transport, steroidogenesis, calcium homeostasis, lipid metabolism, mitochondrial oxidation, cell growth and differentiation, apoptosis induction, and regulation of immune functions.[2,3]

Consistent with its key cellular functions, TSPO is expressed in many peripheral tissues, including liver, heart, kidney, lung, and the immune system, with higher levels appearing in steroid producing tissues.[1,2] In the central nervous system, TSPO normally exists at low level and is mainly located in glial and ependymal cells. Recent evidence suggests that TSPO on glial cells may regulate the biosynthesis of neurosteroids, leading to the hypothesis of a potential role for TSPO in the treatment of neuropathological conditions.[4−7]

TSPO expression is up-regulated in several human pathologies, including gliomas and neurodegenerative disorders (Huntington's and Alzheimer's diseases) as well as in various forms of brain injury and inflammation. Under neuroinflammatory conditions, TSPO markedly increases in activated microglia.[8] Changes in TSPO level have been found in patients affected by generalized anxiety, panic, post-traumatic stress, obsessive−compulsive disorders, and separation anxiety.[4,9,10]

Consequently, TSPO has been suggested as a promising target for a number of therapeutic applications[11] and also as a diagnostic marker for related disease progression, so prompting the development of specific fluorescent[12−14] or radiolabeled[15−17] ligands as powerful tools to image and measure the expression levels of this protein in living cells, isolated tissues, or living subjects. In particular, the use of a selective radioligand with positron emission tomography (PET) allows measurement of the relative density of a target protein in animal and human subjects in vivo. PET studies of TSPO could offer quantitative measures of inflammation, so providing valuable

*To whom correspondence should be addressed. For V.W.P.: phone, +3015945986; fax, +3014805112; E-mail, pikev@mail.nih.gov. For F.D.S.: phone, +390502219561; fax, +390502219605; E-mail, fsettimo@unipi.it.

[a] Abbreviations: ANT, adenine nucleotide translocase; BzR, central benzodiazepine receptor; HABs, high-affinity binders; LABs, low-affinity binders; MABs, mixed-affinity binders; MPTP, mitochondrial permeability transition pore; NCA, no-carrier-added; PET, positron emission tomography; PBR, peripheral benzodiazepine receptor; SA, specific radioactivity; TSPO, translocator protein (18 kDa); VDAC, voltage dependent anion channel.

 Published on Web 12/06/2010 

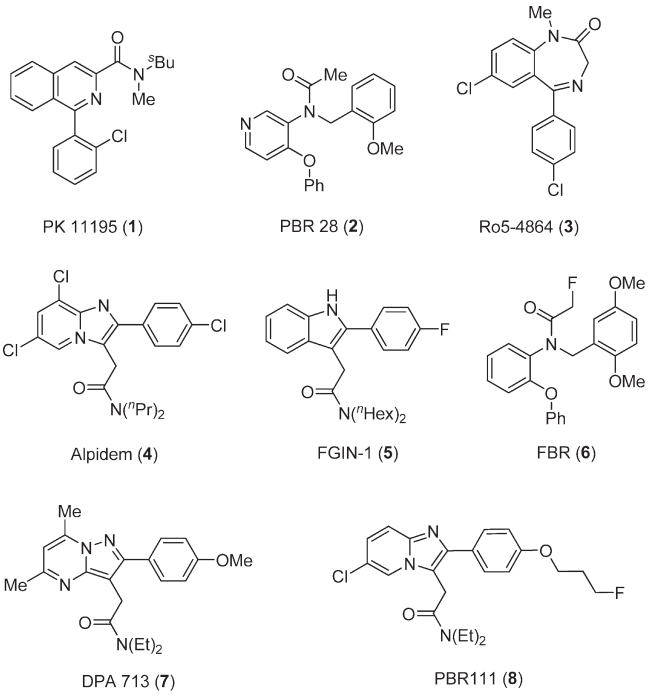


**Figure 1.** Structures of some known TSPO ligands.

biomarker-type measurements during drug development and early clinical trials.[17,18]

[$^{11}$C]PK 11195[19] ([$^{11}$C]**1**; Figure 1), first as racemate[20] and later as *R*-enantiomer,[21] was the first radioligand to be used extensively in the PET imaging of neuroinflammation. However, this radioligand has several limitations, including a high level of nonspecific binding and a poor signal-to-noise ratio which complicate its quantification.[18,22] Therefore, many groups have been searching for TSPO ligands with improved performance for quantifying TSPO expression.[15−17] Recently, more-sensitive radioligands have been introduced for the study of human subjects, including [$^{11}$C]PBR28 ([$^{11}$C]**2**, Figure 1).[22−25] Recent studies with these new radioligands reveal heterogeneity with regard to the form of expression of TSPO in human subjects. For example, in the case of the radioligand [$^{11}$C]**2**, human subjects may be classified as high-affinity binders (HABs), mixed-affinity binders (MABs), or low-affinity binders (LABs).[26] The existence of such different populations, and in particular the more difficult to identify MABs, compromises the accuracy of quantitative comparisons between test and control cohorts. Consequently, there remains a need to find TSPO radioligands that bind with an equally high affinity in all human subjects. One strategy for meeting this need is to explore new chemotypes of TSPO ligand for PET radioligand development.

In recent years, *N*,*N*-dialkyl-(2-phenylindol-3-yl)glyoxylamides (**I**), Figure 2, have been described as a series of potent and selective TSPO ligands, with $K_i$ values in the nanomolar or subnanomolar range; this series represents conformationally constrained analogues of the indoleacetamide derivative, FGIN-1 (**5**) (Figure 1).[27,28]

Within this class, SAR findings were rationalized in the light of the most recently reported pharmacophore/receptor model made up of three lipophilic pockets ($L_1$, $L_3$, and $L_4$) and an H-bond donor group (Figure 2).[27,28] Specifically, the second carbonyl group of the oxalyl bridge engages an H-bond with the donor site $H_1$; the two lipophilic substituents on the amide nitrogen, $R_1$, and $R_2$ (linear or ramified alkyl, arylalkyl groups) interact hydrophobically with the $L_3$ or $L_4$ lipophilic pockets; the 2-phenyl moiety establishes a putative $\pi$-stacking interaction within the $L_1$ pocket (Figure 2).

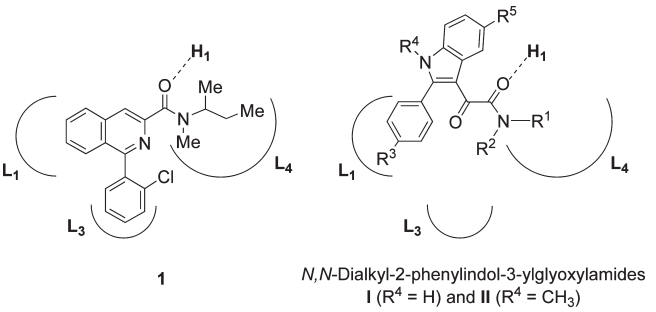


**Figure 2.** Ligand **1** and *N*,*N*-dialkyl-2-phenylindolylglyoxylamides **I** and **II** in the pharmacophore/receptor model of TSPO.[27,28].

**Scheme 1.** Synthesis of New $N^1$-Methyl TSPO Ligands **19**−**31**

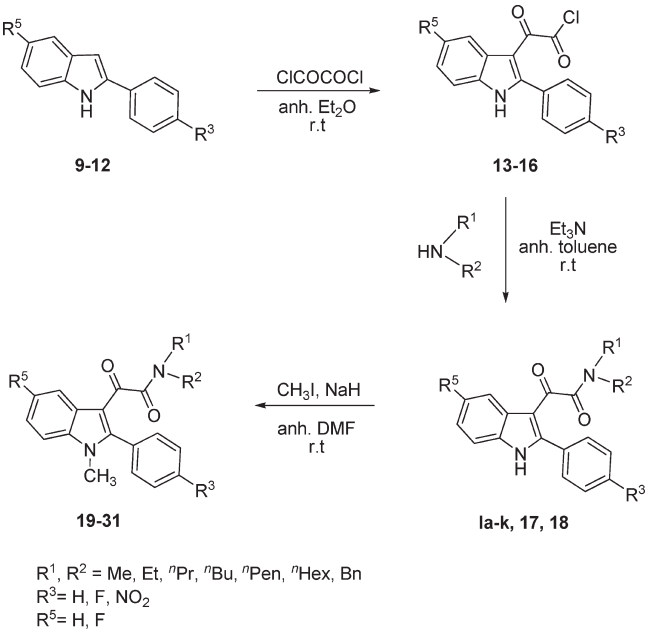


The high affinities of these 2-phenylindolglyoxylamide derivatives **I** have recently permitted the development of new fluorescent probes useful for investigating the localization and the expression level of TSPO.[13,14]

In pursuing our interest in this field, we evaluated the opportunity to develop a novel PET radioligand for TSPO from this chemotype. SAR data and our previously reported pharmacophore/receptor model hypothesis suggested that the indole NH should not be involved in the recognition of the receptor protein (Figure 2). In this view, we developed a small library of novel 2-phenylindol-3-ylglyoxylamide derivatives of general formula **II** (compounds **19**−**31**), featuring a methyl group on the indole nitrogen (Figure 2), as predicted high-affinity TSPO ligands. These compounds, due to the presence of this methyl group, are amenable to labeling with the positron-emitter carbon-11 ($t_{1/2}$ = 20.4 min). Thus, [$^{11}$C]**31** was synthesized and studied for its behavior in monkey in vivo and for the characteristics of its binding to brain membranes collected from a cohort of human subjects.

## Results and Discussion

**Chemistry.** The general procedure for the synthesis of the target *N*,*N*-dialkyl-1-methyl-2-phenylindol-3-ylglyoxylamides

**Table 1.** Physical Properties of *N*,*N*-Dialkylindolylglyoxylamide Derivatives **17**−**31**

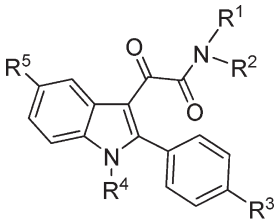

**17**−**31**

| compd | $R^1$ | $R^2$ | $R^3$ | $R^4$ | $R^5$ | yield (%) | mp (°C) | formula[α] |
|---|---|---|---|---|---|---|---|---|
| **17** | Me | Bn | H | H | H | 72 | 98−100 | $C_{24}H_{20}N_2O_2$ |
| **18** | Me | Bn | F | H | H | 89 | 72−74 | $C_{24}H_{19}FN_2O_2$ |
| **19** | $^n$Pr | $^n$Pr | H | Me | H | 90 | 110−112 | $C_{23}H_{26}N_2O_2$ |
| **20** | $^n$Bu | $^n$Bu | H | Me | H | 79 | 83−85 | $C_{25}H_{30}N_2O_2$ |
| **21** | $^n$Hex | $^n$Hex | H | Me | H | 90 | oil | $C_{29}H_{38}N_2O_2$ |
| **22** | Et | $^n$Bu | H | Me | H | 76 | oil | $C_{23}H_{26}N_2O_2$ |
| **23** | Et | Bn | H | Me | H | 70 | oil | $C_{26}H_{24}N_2O_2$ |
| **24** | Me | $^n$Bu | H | Me | H | 64 | 124−126 | $C_{22}H_{24}N_2O_2$ |
| **25** | Me | $^n$Pen | H | Me | H | 70 | 126−128 | $C_{23}H_{26}N_2O_2$ |
| **26** | Me | Bn | H | Me | H | 92 | 148−150 | $C_{25}H_{22}N_2O_2$ |
| **27** | $^n$Pr | $^n$Pr | H | Me | F | 73 | 120−122 | $C_{23}H_{25}FN_2O_2$ |
| **28** | $^n$Pr | $^n$Pr | F | Me | H | 83 | 132−134 | $C_{23}H_{25}FN_2O_2$ |
| **29** | $^n$Hex | $^n$Hex | F | Me | H | 65 | oil | $C_{29}H_{37}FN_2O_2$ |
| **30** | Me | Bn | F | Me | H | 70 | 138−140 | $C_{25}H_{21}FN_2O_2$ |
| **31** | $^n$Pr | $^n$Pr | $NO_2$ | Me | H | 97 | 144−146 | $C_{23}H_{25}N_3O_4$ |

[α] Elemental analyses for C, H, N were within ±0.4% of the calculated values.

**19**−**31** is outlined in Scheme 1 and involved the treatment of previously described **Ia**−**k**[27,28] or newly synthesized indoles (**17** and **18**) with sodium hydride and subsequent addition of an excess of methyl iodide in dry DMF. All products were purified by flash chromatography ($CHCl_3$ as eluent). Their chemical−physical properties were determined (Table 1), and their structures were confirmed by IR, $^1$H NMR, and elemental analysis (Supporting Information). The new compounds, **17** and **18**, were prepared essentially following procedures similar to those used to obtain products **Ia**−**k**,[27,28] as summarized in Scheme 1.

**Binding Affinity on Rat Kidney.** The binding affinity at TSPO of all the newly synthesized indolylglyoxylamides **17**−**31** was determined in rat kidney membranes by binding competition experiments against [$^3$H]**1** as radioligand.[27] Because of the well-established TSPO versus central benzodiazepine receptor (BzR) selectivity of *N*,*N*-dialkyl-2-phenylindol-3-ylglyoxylamides **I**,[27,28] a few randomly selected novel indole derivatives were evaluated for their BzR affinity, using membranes from rat brain tissues and [$^3$H]flumazenil as the radioligand. The tested compounds showed no significant binding properties in this assay (data not shown).

The binding affinities of all the newly synthesized $N^1$-methylated derivatives **19**−**31**, expressed as $K_i$ values, are listed in Table 2, together with those of the standard TSPO ligands **1**, **3**, and **4** (Figure 1). The binding data of some of the parent compounds, **Ia**−**k**,[27,28] and of **17** and **18** are also included for comparison.

All the newly synthesized compounds were found to be potent TSPO ligands, with $K_i$ values in the low nanomolar or subnanomolar range.

The insertion of the methyl group at the $N^1$ position did not significantly influence TSPO binding, as most of the derivatives **19**−**31** showed $K_i$ values ranging from 0.3 to 60 nM, essentially comparable with those of their unsubstituted

**Table 2.** TSPO Binding Affinity of *N*,*N*-Dialkylindolylglyoxylamide Derivatives **Ia**−**k**, and **17**−**31**

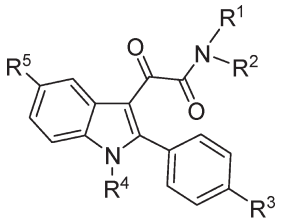

**Ia**−**k, 17**−**31**

| ligand | $R^1$ | $R^2$ | $R^3$ | $R^4$ | $R^5$ | $K_i$ (nM)[a] |
|---|---|---|---|---|---|---|
| **1** | | | | | | 9.30 ± 0.50 |
| **3** | | | | | | 23.0 ± 3.0 |
| **4** | | | | | | 0.5−7 |
| **Ia**[b] | $^n$Pr | $^n$Pr | H | H | H | 12.2 ± 1.0 |
| **Ib**[b] | $^n$Bu | $^n$Bu | H | H | H | 7.50 ± 0.70 |
| **Ic**[b] | $^n$Hex | $^n$Hex | H | H | H | 1.40 ± 0.20 |
| **Id**[c] | Et | $^n$Bu | H | H | H | 12.6 ± 1.0 |
| **Ie**[c] | Et | Bn | H | H | H | 11.0 ± 1.0 |
| **If**[c] | Me | $^n$Bu | H | H | H | 53.3 ± 4.0 |
| **Ig**[c] | Me | $^n$Pen | H | H | H | 12.1 ± 1.0 |
| **17** | Me | Bn | H | H | H | 12.0 ± 1.0 |
| **Ih**[c] | $^n$Pr | $^n$Pr | H | H | F | 2.67 ± 0.48 |
| **Ii**[b] | $^n$Pr | $^n$Pr | F | H | H | 4.28 ± 0.32 |
| **Ij**[b] | $^n$Hex | $^n$Hex | F | H | H | 0.370 ± 0.13 |
| **18** | Me | Bn | F | H | H | 1.80 ± 0.10 |
| **Ik**[c] | $^n$Pr | $^n$Pr | $NO_2$ | H | H | 0.950 ± 0.10 |
| **19** | $^n$Pr | $^n$Pr | H | Me | H | 19.5 ± 1.5 |
| **20** | $^n$Bu | $^n$Bu | H | Me | H | 0.300 ± 0.050 |
| **21** | $^n$Hex | $^n$Hex | H | Me | H | 0.299 ± 0.050 |
| **22** | Et | $^n$Bu | H | Me | H | 60.2 ± 6.0 |
| **23** | Et | Bn | H | Me | H | 2.92 ± 0.30 |
| **24** | Me | $^n$Bu | H | Me | H | 190 ± 10 |
| **25** | Me | $^n$Pen | H | Me | H | 38.2 ± 4.0 |
| **26** | Me | Bn | H | Me | H | 20.9 ± 1.8 |
| **27** | $^n$Pr | $^n$Pr | H | Me | F | 23.7 ± 2.1 |
| **28** | $^n$Pr | $^n$Pr | F | Me | H | 19.8 ± 2.0 |
| **29** | $^n$Hex | $^n$Hex | F | Me | H | 1.07 ± 0.11 |
| **30** | Me | Bn | F | Me | H | 6.77 ± 0.50 |
| **31** | $^n$Pr | $^n$Pr | $NO_2$ | Me | H | 5.70 ± 0.45 |

[a] The concentration of tested compounds that inhibited [$^3$H]**1** binding to rat kidney mitochondrial membranes by 50% ($IC_{50}$) was determined with six concentration of the displacers, each performed in triplicate. $K_i$ values are the mean ± SEM of three determinations. [b] Data taken from ref 27. [c] Data taken from ref 28.

counterparts **Ia**−**k**, **17**, and **18**. The only exception was compound **24**, which showed a low affinity ($K_i$ 190 nM). Compounds **20** and **21** possessed the highest affinity in this series ($K_i$ 0.30 nM) and a 25- and 4.6-gain in activity with respect to their desmethyl counterparts, **Ib** and **Ic**, respectively. These results agree with our previously reported pharmacophore/receptor model hypothesis, where the indole NH is not involved in the recognition of the receptor protein.

**Radioligand Synthesis.** The high affinity of the newly synthesized $N^1$-methylated-2-phenylindol-3-ylglyoxylamide derivatives **19**−**31** made them good candidates for the development of radioligands for the imaging of TSPO. The choice of the best candidate to be labeled with carbon-11 was guided by two main factors, namely adequate high affinity toward TSPO and suitably moderate lipophilicity for achieving adequate brain entry and low nonspecific binding.[29−32] On the basis of these two parameters, we selected **31** as the ligand from the new series showing the best combination of affinity

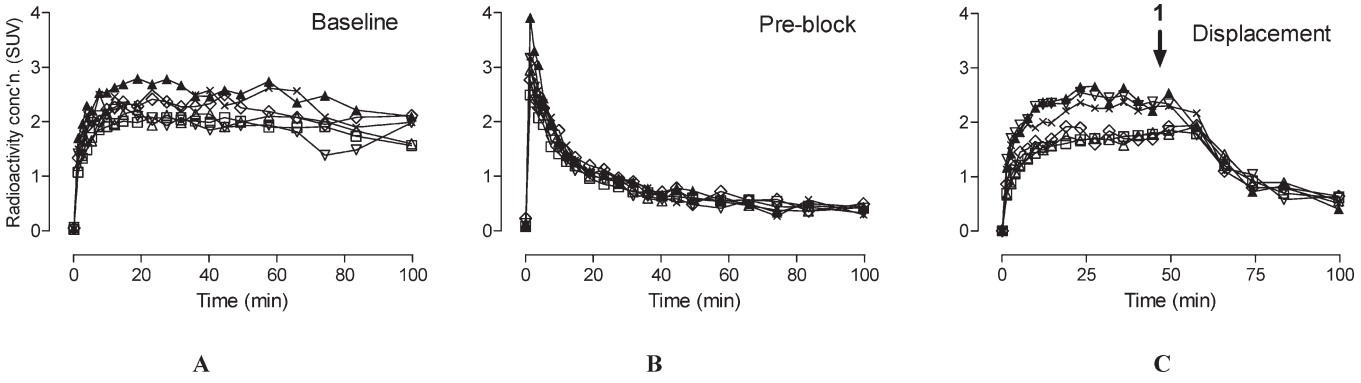


**Figure 3.** Brain region time−activity curves in monkey after injection of [$^{11}$C]**31** in (A) a baseline (radioligand alone) experiment, (B) a TSPO preblock experiment in which the TSPO ligand **1** (5 mg/kg, iv) was given at 10 min before radioligand, and (C) a displacement experiment in which **1** (5 mg/kg, iv) was given at 48 min after radioligand. Key: Anterior cingulate (△), cerebellum (▽), hippocampus (◇), prefrontal cortex (□), putamen (▲), and thalamus (×).

($K_i$ 5.7 nM) and lipophilicity (cLogP 3.95) to be labeled with carbon-11 and evaluated as a TSPO radioligand in vivo.

[$^{11}$C]**31** was rapidly prepared by treating the *N*-desmethyl analogue **1k** with [$^{11}$C]methyl iodide and solid KOH in DMSO and purified by HPLC preceding formulation for intravenous injection. [$^{11}$C]**31** was obtained in high radiochemical purity (>99%), chemical purity, and specific radioactivity (typically >4 Ci/$\mu$mol at end of synthesis) and was radiochemically stable. Adequate activities (>25 mCi) were readily obtained for PET imaging in monkey.

**PET Imaging of [$^{11}$C]31 in Monkeys.** The ability of [$^{11}$C]**31** to image brain TSPO in vivo was tested with PET in rhesus monkeys. After injection of no-carrier-added (NCA) [$^{11}$C]**31** into monkeys, radioactivity entered the brain well, with peak radioactivity uptake occurring in all TSPO-containing regions by about 40 min after injection (Figure 3A). Maximal uptake occurred in putamen (2.32 ± 0.72, SUV; $n$ = 7) between 12 and 32 min after injection. This moderately high uptake is comparable to that achieved with other prominent TSPO radioligands such as [$^{11}$C]**2**[23] and [$^{18}$F]**6**[33] (Figure 1). Subsequent washout of radioactivity from all TSPO-containing regions was quite slow. In repeating the experiments in three monkeys in which TSPO receptors were preblocked by administration of **1** (5 mg/kg, iv), the kinetics of brain radioactivity was strikingly different. Radioactivity was rapidly taken into all examined brain regions to a higher level than in the baseline experiment and then washed out rapidly to a low common level (Figure 3B). In a displacement experiment in another monkey, administration of **1** (5 mg/kg, iv) at 48 min after radioligand caused a rapid decline in radioactivity in all TSPO-containing regions to a low common level (Figure 3C). These data show the presence of a high proportion of specific binding of radioligand to brain TSPO in the baseline experiments and furthermore demonstrate the reversibility of this binding.

Average PET images of monkey brain acquired over 4−100 min after injection of [$^{11}$C]**31** (Figure 4) displayed a high level of radioactivity, especially in putamen, cerebellum, and intermediate levels in cortical regions. Scans from the corresponding preblock experiments showed a very uniform low distribution of radioactivity, consistent with absence of radioligand specific binding (Figure 4).

**Emergence of Radiometabolites of [$^{11}$C]31 in Monkey Plasma In Vivo.** Generally, PET radioligands are appreciably metabolized over the short time span of a PET scanning session. Detailed quantitative analysis of radioligand behavior in vivo to

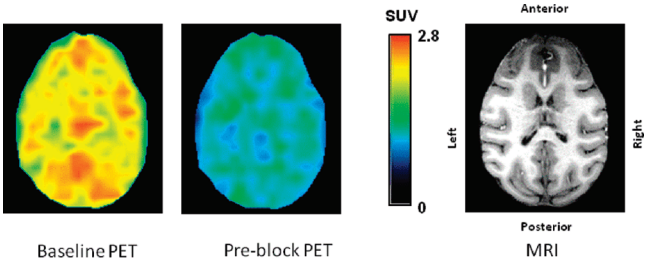


**Figure 4.** Horizontal PET images of monkey brain at the level of the caudate acquired between 4 and 100 min after intravenous injection of monkey with [$^{11}$C]**31** under baseline and preblock conditions and corresponding MRI scan.

derive important output measures such as binding potential or volume of distribution may require measurement of the free fraction of radioligand in plasma ($f_P$) and also a determination of the amount of unmetabolized radioligand in plasma over the full duration of a scanning session. Generally, PET radioligands which produce brain-penetrant radiometabolites are often difficult to quantify.[30,31] [$^{11}$C]**31** was stable in monkey whole blood and in buffer in vitro. The plasma free fraction of [$^{11}$C]**31** in monkey blood in vitro was low (0.71 ± 0.13%; $n$ = 3), in accordance with the moderately high lipophilicity of **31** (cLogP = 3.95). After administration of [$^{11}$C]**31** into monkey, both the total radioactivity in plasma and the parent radioligand component reduced rapidly (Figure 5). Recoveries of radioactivity from plasma into supernatant acetonitrile for HPLC analysis exceeded 94%. HPLC analyses of plasma from monkeys studied at baseline revealed [$^{11}$C]**31** eluting at 5.18 ± 1.41 min, and three less lipophilic radiometabolites [$^{11}$C]**A**−[$^{11}$C]**C** eluting at 2.02 ± 0.60, 2.79 ± 0.80, and 3.71 ± 0.95 min ($n$ = 96), respectively. Monkey plasma radioactivity became composed equally of radiometabolites and [$^{11}$C]**31** at 38.8 and 80.8 min in two baseline experiments and at 7.8 and 17.5 min in TSPO-preblock experiments in the same monkeys, respectively (Figure 5). A greater availability of TSPO-free radioligand for metabolism in the preblock experiments may account for the more rapid appearance of radiometabolites in the preblock experiments. The identities of the three radiometabolites are currently unknown, as is their ability to penetrate the blood−brain barrier. Their lower lipophilicity relative to the radioligand may however render them less brain-penetrant and relatively untroublesome to quantitative analysis.

The concentration of unchanged [$^{11}$C]**31** in plasma (SUV) was appreciably higher in TSPO preblock experiments than

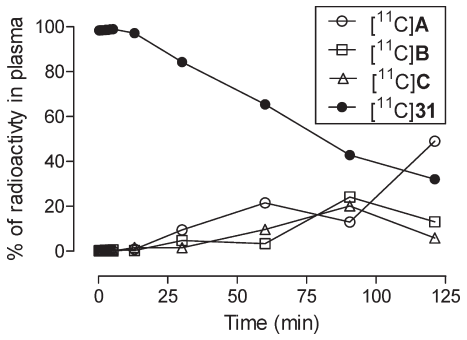


**Figure 5.** Emergence of three radiometabolites, [$^{11}$C]**A**−[$^{11}$C]**C**, of [$^{11}$C]**31** in plasma of one monkey under baseline conditions.

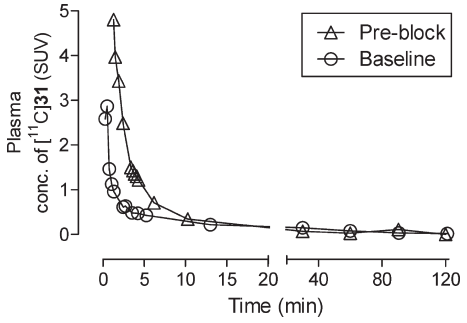


**Figure 6.** Time-course of concentration of unmetabolized [$^{11}$C]**31** in plasma after intravenous injection into monkey under baseline and preblocked conditions.

in baseline experiments, especially over the initial 10 min (Figure 6). Such increases have also been seen for other radioligands[23,33] and are attributed to the prevention of radioligand binding to abundant TSPO receptors in peripheral organs by the administered TSPO preblocking agent. In this regard, whole body PET scanning of a monkey before and after treatment with **1** clearly showed displacement of activity from TSPO-containing organs such as liver, lung, heart, kidney, and spleen with a concomitant increase in radioactivity in bladder (see Supporting Information).

**Binding of Ligand 31 to Human Brain Tissue.** Ligand **31** showed similar high-affinity brain tissue binding in "high-affinity binders; HABs" ($K_i$ = 1.57 ± 1.03 nM, $n$ = 4) and "mixed-affinity binders; MABs" ($K_i$ = 1.82 ± 1.09 nM, $n$ = 4) and somewhat lower affinity in "low-affinity binders; LABs" ($K_i$ = 9.53 ± 6.25 nM, $n$ = 5) (Figure 7). The differences in affinity toward LABs versus HABs or MABs are statistically significant ($P < 0.05$ for both HABs and MABs). However, these differences in $K_i$ should be treated with some caution because they may reflect possible differences in the affinity of binding of the reference radioligand ([$^3$H]**1**) toward HABs, MABs and LABs. Although ligand **31** appears to show some sensitivity to LABs, sensitivity to MABs versus HABs is less clear from the small number of tests (and is statistically insignificant, $P$ = 0.250). If, as suggested by Owen et al.,[34] that the MABs have about a 1:1 mixture of the high-affinity and low-affinity binding sites, then by the Cheng−Prusoff equation,[35] the affinity expected for **31** in the MABs should be about 2-fold lower than in the HABs. The data here, from only 4 HABs and 4 MABs, indicate they have similar affinities. Binding data in a larger group of subjects, preferably with tritiated **31** as radioligand, are needed to clarify whether true differences in binding affinities exist between HABs and MABs.

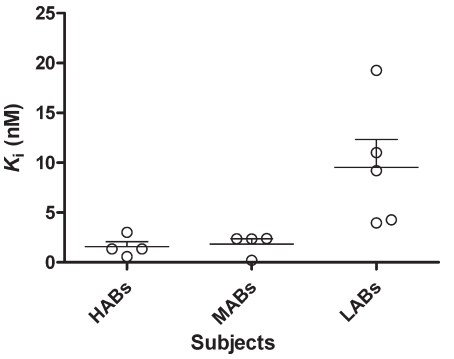


**Figure 7.** $K_i$ values of **31** for brain tissue TSPO from human "high-affinity binders, HABs", "mixed-affinity binders, MABs", and "low-affinity binders, LABs". Each point is from a single human subject.

## Summary

In this study, a novel series of 2-phenylindol-3-ylglyoxylamides featuring a $N^1$-methyl substituent was developed. When tested on rat kidney membranes, most of the new compounds showed high affinity for TSPO, with $K_i$ values comparable to those of their $N^1$-unsubstituted parent derivatives, in accordance with our previously reported pharmacophore/topological model hypothesis, where the indole NH is not involved in the recognition of the receptor protein. Thus, $N^1$-methyl-2-phenylindol-3-ylglyoxylamides constitute a new chemotype of high-affinity TSPO ligands with potential for development to produce effective radioligands for imaging brain TSPO with PET, of which [$^{11}$C]**31** is the first example. [$^{11}$C]**31** was easily prepared and readily entered monkey brain to give a high proportion of reversible specific binding to TSPO. As for other chemotypes,[26,34] such as the aryloxyanilides, exemplified by **2** and **6**, and the linked bicyclics, exemplified by DPA713 (**7**) and PBR111 (**8**) (Figure 1),[26,34] this new chemotype shows different affinity for the two forms of brain TSPO found among human subjects. However, the difference in affinities is quite small compared to that of the aryloxyanilide **2** and indicates the possibility to find a new PET radioligand from this structural class with a truly insignificant difference that will be applicable in all human subjects.

## Experimental Section

**Materials and Methods.** All reagents used were obtained from commercial sources (Sigma-Aldrich). All solvents were of an analytical grade. 2-Phenylindole (**9**) and 2-(4-fluorophenyl)indole (**10**) were from Sigma-Aldrich. 5-Fluoro-2-phenylindole (**11**), 2-(4-nitrophenyl)indole (**12**), 2-phenylindol-3-ylglyoxyl chloride (**13**), 2-(4-fluorophenyl)indol-3-ylglyoxylchloride (**14**), 5-fluoro-2-phenylindol-3-ylglyoxyl chloride (**15**), and 2-(4-nitrophenyl)indol-3-ylglyoxylchloride (**16**) were prepared as previously described.[27,28] **1** and **3** were obtained from Sigma-Aldrich. Racemic [$^3$H]**1** (SA, 84.8 Ci/mmol) and [$^3$H]flumazenil (SA, 83.4 Ci/mmol) were purchased from Perkin-Elmer Life Sciences.

Melting points were determined using a Reichert Köfler hot-stage apparatus and are uncorrected. Infrared spectra were recorded with a Nicolet-Avatar 360 FT-IR spectrophotometer in Nujol mulls. Routine nuclear magnetic resonance spectra were recorded in DMSO-$d_6$ solution on a Gemini 200 spectrometer (Varian) operating at 200 MHz. Evaporation was performed in vacuo (rotary evaporator). Analytical TLC was carried out on 0.2 mm precoated silica gel aluminum sheets (60 F-254; Merck). Silica gel 60 (230−400 mesh) was used for column chromatography. Combustion analyses on target compounds were performed by our Analytical Laboratory in Pisa. All compounds showed ≥95% purity.

$\gamma$-Radioactivity from $^{11}C$ was measured using a calibrated dose calibrator (Atomlab 300; Biodex Medical Systems). Radioactivity measurements were corrected for physical decay. All radiochemistry was performed in lead-shielded hot cells for personnel protection from radiation.

**General Procedure for the Synthesis of *N*,*N*-Dialkyl-2-(phenylindol-3-yl)glyoxylamide Derivatives 17−18.** Oxalyl chloride (0.65 mL, 7.5 mmol) was added dropwise at 0 °C to a well-stirred mixture of the appropriate indole **9** or **10** (3.0 mmol) in freshly distilled diethyl ether (10 mL). The mixture was maintained at room temperature for 2−24 h (TLC analysis). The generated precipitate was collected and washed with portions of anhydrous diethyl ether to give the acyl chlorides **13** or **14**[27,28] which were dried over $P_2O_5$ in vacuo and then suspended in 50 mL of dry toluene. A solution of *N*-benzyl-*N*-methylamine (0.30 mL, 2.5 mmol) in dry toluene (5 mL) was then added dropwise, at 0 °C, followed by the addition of a solution of triethylamine (0.3 mL, 2.5 mmol) in the same solvent (5 mL). The reaction mixture was allowed to warm to room temperature, stirred for 2−24 h (TLC analysis), and then filtered. The collected precipitate was triturated with a saturated $NaHCO_3$ aqueous solution, washed with water, and collected again to give a first portion of crude product. The toluene solution was evaporated to dryness, and the residue was treated with saturated $NaHCO_3$ aqueous solution, washed with water, and collected to yield an additional amount of crude product. The quantities of amide derivatives obtained from the initial insoluble precipitate or from the toluene solution were variable, depending upon the solubility of the various compounds. Products **17** and **18** were purified by flash chromatography ($CHCl_3$ as eluent). Yields and melting points of compounds **17** and **18** are listed in Table 1; spectral data are reported in the Supporting Information.

**General Procedure for the Synthesis of *N*,*N*-Dialkyl-1-methyl-2-phenylindol-3-ylglyoxylamides Derivatives, 19−31.** Sodium hydride (0.11 mmol, 50% dispersion in mineral oil) was added portionwise, under a nitrogen atmosphere, to an ice-cooled solution of the appropriate *N*,*N*-dialkyl-2-phenylindol-3-ylglyoxylamide derivative **Ia−k**,[27,28] **17**, and **18** (0.1 mmol) in dry DMF (3 mL). Once hydrogen evolution had ceased, an excess of methyl iodide (0.018 mL, 0.3 mmol) was quickly added at 0 °C. The reaction was maintained under stirring at room temperature until the disappearance of the starting material (12−24 h, TLC analysis). The solvent was eliminated under vacuum, and the residue was triturated with crushed ice and filtered or extracted ($CHCl_3$). The products were finally purified by flash chromatography ($CHCl_3$ as eluent). Yields and melting points of compounds **19−31** are listed in Table 1; spectral data are reported in the Supporting Information.

**Inhibition of [$^3$H]1 Binding to Rat Kidney Mitochondrial Membranes.** For binding studies, crude mitochondrial membranes were incubated with [$^3$H]**1** (0.6 nM) in the presence of a test compound in the concentration range (0.05 nM−10 $\mu$M) in Tris-HCl buffer (50 mM, pH 7.4) as previously described.[27] For the active compounds, the $IC_{50}$ values were determined and $K_i$ values were derived in accordance with the Cheng−Prusoff equation.[35]

**Inhibition of [$^3$H]Flumazenil Binding to Rat Cerebral Cortex Membranes.** Rat cerebral cortex membranes were prepared as previously described.[36] After differential centrifugation, the obtained crude membrane fraction was subjected to washing procedures to remove endogenous GABA.[37] The washed membranes were incubated with [$^3$H]flumazenil (0.4 nM) for 90 min at 0 °C in Tris-citrate buffer (50 mM, 500 $\mu$L, pH 7.4), as previously described.[38]

**Radiochemistry. Production of NCA [$^{11}$C]Carbon Dioxide.** No-carrier-added (NCA) [$^{11}$C]carbon dioxide (~2.3 Ci) was produced with a PETtrace cyclotron (GE Medical Systems; Milwaukee, WI) according to the $^{14}N(p,\alpha)^{11}C$ reaction[39] by irradiation of nitrogen gas (initial pressure 160 psi; 75-mL volume) containing 1% oxygen with a proton beam (16.5 MeV, 45 $\mu$A) for 40 min.

**Production of NCA [$^{11}$C]Methyl Iodide.** NCA [$^{11}$C]methyl iodide was produced from NCA [$^{11}$C]carbon dioxide via reduction to [$^{11}$C]methane and then vapor phase iodination.[40] Thus, at the end of the proton irradiation, [$^{11}$C]carbon dioxide was delivered to a PETtrace MeI process module (GE Medical Systems, model KAB301-31001) inside a hot cell through stainless tubing (OD $^1/_8$ in, ID $^1/_{16}$ in) over 2 min and trapped on molecular sieve (13×) and reduced to [$^{11}$C]methane over nickel at 360 °C. The [$^{11}$C]methane was recirculated over iodine at 720 °C to generate [$^{11}$C]methyl iodide, which was trapped on Porapak Q held in the recirculation path.

**Labeling of 31 with Carbon-11.** Compound **1k** (0.5 mg) was added to a V-vial containing anhydrous DMSO (0.4 mL) containing finely ground KOH (4 mg). [$^{11}$C]Methyl Iodide was released from the Porapak trap at 180 °C into a stream of nitrogen and bubbled into the DMSO at 17 mL/min until the radioactivity in the vial maximized. The mixture was then heated at 80 °C for 5 min, after which the crude reaction mixture was diluted with water (500 $\mu$L). The product was injected onto a Gemini C18 column (5 $\mu$m, 10 mm × 250 mm; Phenomenex) eluted at 6 mL/min with a mobile phase of MeCN-0.1M aq $HCOONH_4$ initially composed of 50% MeCN and increased linearly to 80% MeCN over 10 min. Eluate was monitored for absorbance at 254 nm (Beckman 166 UV detector) and for $\gamma$-radiation with a semiconductor pin-diode detector (Bioscan). [$^{11}$C]**31** ($t_R$ = 10 min) was collected and mobile phase and ammonium formate removed under high vacuum at 80 °C. Ethanol (1.5 mL) was added to dissolve the radioactive residue and the solution then diluted with saline (13.5 mL). Finally, this solution was sterilized by filtration through a sterile MP filter to provide [$^{11}$C]**31** ready for intravenous injection, pending HPLC analysis.

[$^{11}$C]**31** was analyzed for radiochemical purity, specific activity, and chemical purity with HPLC on a Luna C18 column (5 $\mu$m, 4.6 mm × 250 mm) eluted with MeCN-0.1 M aq $HCOONH_4$ (60: 40 v/v) at 3.0 mL/min. Eluates were monitored for radioactivity (pin-diode detector; Bioscan) and absorbance at 254 nm. Samples were injected alone and then coinjected with the reference nonradioactive compound to check for coelution. The identity of the product was further confirmed by LC/MS/MS of associated carrier on a Finnigan LCQ deca instrument.

**Computation of cLogP.** cLogP for **31** was computed with ChemDraw.

**PET Experiments with [$^{11}$C]31 in Monkeys.** All animals were handled in accordance with the *Guide for the Care and Use of Laboratory Animals*[41] and the National Institute of Health Animal Care and Use Committee. For each scanning session, the subject monkey was immobilized with ketamine and maintained under anesthesia with 1−3% isoflurane in oxygen. An intravenous perfusion line filled with saline (0.9% w/v) was used for bolus injection of [$^{11}$C]**31** of 99.9% radiochemical purity. Dynamic PET images of brain radioactivity were obtained for up to 100 min on an Advance (GE Medical Systems, WI) PET camera.

Decay-corrected time−activity curves (TACs) were obtained for irregular volumes of interest (VOIs) in brain, selected from prefrontal cortex, temporal cortex, parietal cortex, occipital cortex, hippocampus, striatum, thalamus, and cerebellum. Radioactivity levels in VOIs were normalized for injected dose and monkey weight and expression as a standardized uptake value (SUV):

$$\text{SUV} = [(\%\text{injected dose per g tissue}) \times (\text{body weight in g})]/100$$

The following scans were performed among four monkeys. Baseline scans: All four male rhesus (*Mucacca mulatto*) monkeys (6.4−12.0 kg) received brain scans at baseline after bolus intravenous injection of [$^{11}$C]**31** (4.76−6.70 mCi; dose of **31**,

0.155−0.859 nmol/kg). TSPO preblock scans: Two monkeys (11.1 and 12 kg) were scanned with [$^{11}$C]**31** (6.10 and 6.40 mCi; dose of **31**, 0.108 and 0.135 nmol/kg of **31**) at 10 min after administration of the TSPO ligand **1** (5 mg/kg, iv). TSPO displacement scan: One monkey (12.82 kg) was scanned with [$^{11}$C]**31** (5.60 mCi; dose of **31**, 0.156 nmol/kg) with **1** (5 mg/kg, iv) administered over 2 min at 48 min from the start of the scan.

**Stability of [$^{11}$C]31 in Monkey Whole Blood in Vitro, and in Buffer.** [$^{11}$C]**31** was incubated for 45 min in whole monkey blood (1 mL). A sample (0.5 mL) was removed, added to acetonitrile (0.8 mL), and centrifuged. Then the supernatant liquid was analyzed by reverse phase radio-HPLC. The stability of [$^{11}$C]**31** to incubation in sodium phosphate buffer (0.15 M, pH 7.4) for 2 h at room temperature was also assessed by reverse phase HPLC.

**Plasma Protein Binding of [$^{11}$C]31.**[42] The radioligand was added to pooled human plasma, placed at the top of an "Amicon" Centrifree filter unit (200 $\mu$L/unit) and filtered by ultra centrifugation at 5000*g*. Then all components of filter units were counted for radioactivity to allow calculation of radioligand plasma protein binding ($f_P$).

**Emergence of Radiometabolites of [$^{11}$C]31 in Monkey Plasma In Vivo.** During each of four PET scans (two baseline and two preblock), blood samples were drawn periodically from the monkey femoral artery and collected in heparin-treated Vacutainer tubes. The samples were centrifuged and the plasma separated. A sample of plasma (0.45 mL) was mixed with acetonitrile (0.72 mL) and centrifuged. The supernatant liquid was analyzed with radio-HPLC on a Novapak C18 column (4 $\mu$m; 8 mm × 100 mm) eluted at 2.0 mL/min with MeOH/$H_2O$/$Et_2O$ (75: 25: 0.1 by vol.). The time courses for percentages of radioactivity in plasma represented by [$^{11}$C]**31** and its radiometabolites were calculated.

**Human Brain Membrane Preparation.** Human brain tissue from 13 donors was obtained from the UK National Multiple Sclerosis (MS) Brain Bank. Ethical approval for the study procedures was granted by the local Research Ethics Committee (Imperial College). Four of these donors had been classified previously, through ethically approved in vitro studies, as high-affinity binders (HABs) for the TSPO ligand **2**, four as mixed-affinity binders (MABs) and five as low-affinity binders (LABs).[26] Donor tissue blocks were homogenized in 10 times weight for volume buffer (0.32 mM sucrose, 5 mM Tris-Base, 1 mM $MgCl_2$, pH 7.4, 4 °C). Homogenates were centrifuged (32000*g*, 20 min, 4 °C) followed by removal of the supernatant. Pellets were resuspended in at least 10 times w/v (weight for volume) buffer (50 mM Tris-Base, 1 mM $MgCl_2$, pH 7.4, 4 °C), followed by two washes by centrifugation (32000*g*, 20 min, 4 °C). Membranes were suspended in buffer (50 mM Tris-Base, 1 mM $MgCl_2$, pH 7.4, 4 °C) at a protein concentration of about 4 mg protein/mL and aliquots were stored at −80 °C until use.

**Human Brain Homogenate and Competition Binding Assays.** Aliquots (about 250 mg protein/mL) of membrane suspension were prepared using assay buffer (50 mM Tris-Base, 140 mM NaCl, 1.5 mM $MgCl_2$, 5 mM KCl, 1.5 mM $CaCl_2$, pH 7.4, 37 °C) and incubated with [$^3$H]**1** (5 nM) and one of 11 concentrations of unlabeled **31** ranging from 0.03 nM to 10 $\mu$M at 37 °C in a final volume of 500 $\mu$L for 60 min. The specific binding component was defined by addition of unlabeled **1** (10 mmol/L). After incubation, assays were terminated by filtration through GF/B filters (Whatman, Maidstone, UK), followed by 3 × 1 mL washes with ice-cold wash buffer (50 mM Tris-Base, 1.4 mM $MgCl_2$, pH 7.4, 4 °C). GF/B filters were preincubated with 0.05% polyethyleneimine (60 min) before filtration. Scintillation fluid (3 mL/vial, Perkin-Elmer Ultima Gold MV) was added and vials counted on a Perkin-Elmer Tricarb 2900 liquid scintillation counter. Each point was performed in quadruplicate. $K_i$ (nM) values were determined with GraphPad Prism 5.0 software (GraphPad Software Inc., La Jolla, CA, USA).

**Acknowledgment.** This study was supported by the Intramural Research Program of the National Institutes of Health (NIH), specifically the National Institute of Mental Health (NIMH), and the Tuscan Cancer Institute (Istituto Toscano Tumori, ITT, grant 2007). We thank the UK Multiple Sclerosis Tissue Bank (Director, Prof. Richard Reynolds) for providing human brain tissue samples used in this study. We also thank the NIH PET Department for radioisotope production and Kimberley J. Jenko and Kacey B. Anderson for assistance with blood analysis.

**Supporting Information Available:** Table collecting spectral data of compounds **17**−**31** and a table of analytical data of compounds **17**−**31**. Whole-body PET scan of monkey at baseline and after TSPO block. This material is available free of charge via the Internet at http://pubs.acs.org.

## References

(1) Papadopoulos, V.; Baraldi, M.; Guilarte, T. R.; Knudsen, T. B.; Lacapere, J. J.; Lindemann, P.; Norenberg, M. D.; Nutt, D.; Weizman, A.; Zhang, M.; Gavish, M. Translocator protein (18 kDa): new nomenclature for the peripheral-type benzodiazepine receptor based on its structure and molecular function. *Trends Pharmacol. Sci.* **2006**, *27*, 402–409.

(2) Casellas, P.; Galiegue, S.; Basile, A. S. Peripheral benzodiazepine receptors and mitochondrial function. *Neurochem. Int.* **2002**, *40*, 475–486.

(3) Rone, M. B.; Ran, J.; Papadopoulos, V. Cholesterol transport in steroid biosynthesis: role of protein−protein interactions and implications in disease states. *Biochim. Biophys. Acta* **2009**, *1791*, 646–658.

(4) Papadopoulos, V.; Lecanu, L.; Brown, R. C.; Han, Z.; Yao, Z.-X. Peripheral-type benzodiazepine receptor in neurosteroid biosynthesis, neuropathology and neurological disorders. *Neuroscience* **2006**, *138*, 749–756.

(5) Taliani, S.; Da Settimo, F.; Da Pozzo., E.; Chelli, B.; Martini, C. Translocator protein ligands as promising therapeutic tools for anxiety disorders. *Curr. Med. Chem.* **2009**, *16*, 3359–3380.

(6) Veenman, L.; Gavish, M. Peripheral benzodiazepine receptors: their implication in brain disease. *Drug. Dev. Res.* **2000**, *50*, 355–370.

(7) Rupprecht, R.; Rammes, G.; Eser, D.; Baghai, T. C.; Schule, C.; Nothdurfter, C.; Troxler, T.; Gentsch, C.; Kalkman, H. O.; Chaperon, F.; Uzunov, V.; McAllister, K. H.; Bertaina-Anglade, V.; Drieu La Rochelle, C.; Tuerck, D.; Floesser, A.; Kiese, B.; Schumacher, M.; Landgraf, R.; Holsboer, F.; Kucher, K. Translocator protein (18 kDa) as target for anxiolytics without benzodiazepine-like side effects. *Science* **2009**, *325*, 490–493.

(8) Chen, M.-K; Guilarte, T. R. Translocator protein 18 kDa (TSPO): molecular sensor of brain injury and repair. *Pharmacol. Ther.* **2008**, *118*, 1–17.

(9) Chelli, B.; Pini, S.; Abelli, M.; Cardini, A.; Lari, L.; Muti, M.; Gesi, C.; Cassano, G. B.; Lucacchini, A.; Martini, C. Platelet 18 kDa translocator protein density is reduced in depressed patients with adult separation anxiety. *Eur. Neuropsychopharmacol.* **2008**, *18*, 249–254.

(10) Dell'Osso, L.; Da Pozzo, E.; Carmassi, C.; Trincavelli, M. L.; Ciapparelli, A.; Martini, C. Lifetime manic−hypomanic symptoms in post-traumatic stress disorder: relationship with the 18 kDa mitochondrial translocator protein density. *Psychiatry Res.* **2010**, *177*, 139–143.

(11) Galiegue, S.; Tinel, N.; Casellas, P. The peripheral benzodiazepine receptor: a promising therapeutic drug target. *Curr. Med. Chem.* **2003**, *10*, 1563–1572.

(12) Laquintana, V.; Denora, N.; Lopedota, A.; Suzuki, H.; Sawada, M.; Serra, M.; Biggio, G.; Latrofa, A.; Trapani, G.; Liso, G. *N*-Benzyl-2-(6,8-dichloro-2-(4-chlorophenyl)imidazo[1,2-*a*]pyridin-3-yl)-*N*-(6-(7-nitrobenzo[*c*][1,2,5]oxadiazol-4-ylamino)hexyl)acetamide as a new fluorescent probe for peripheral benzodiazepine receptor and microglial cell visualization. *Bioconjugate Chem.* **2007**, *18*, 1397–1407.

(13) Taliani, S.; Simorini, F.; Sergianni, V.; La Motta, C.; Da Settimo, F.; Cosimelli, B.; Abignente, E.; Greco, G.; Novellino, E.; Rossi, L.; Gremigni, V.; Spinetti, F.; Chelli, B.; Martini, C. New fluorescent 2-phenylindolglyoxylamide derivatives as probes targeting the peripheral-type benzodiazepine receptor: design, synthesis, and biological evaluation. *J. Med. Chem.* **2007**, *50*, 404–407.

(14) Taliani, S.; Da Pozzo, E.; Bellandi, M.; Bendinelli, S.; Pugliesi, I.; Simorini, F.; La Motta, C.; Salerno, S.; Marini, A. M.; Da Settimo, F.; Cosimelli, B.; Greco, G.; Novellino, E.; Martini, C. Novel irreversible fluorescent probes targeting the 18 kDa translocator protein: synthesis and biological characterization. *J. Med. Chem.* **2010**, *53*, 4085–4093.
(15) Schweitzer, P. J.; Fallon, B. A.; Mann, J. J.; Kumar, J. S. D. PET tracers for the peripheral benzodiazepine receptor and uses thereof. *Drug Discovery Today* **2010**, *15*, 933–942.
(16) Dollé, F.; Luus, C.; Reynolds, A.; Kassiou, M. Radiolabelled molecules for imaging the translocator protein (18 kDa) using positron emission tomography. *Curr. Med. Chem.* **2009**, *16*, 2899–2923.
(17) Chaveau, F.; Boutin, H.; Van Camp, N.; Dollé, F.; Tavitian, B. Nuclear imaging of neuroinflammation: a comprehensive review of [$^{11}$C]PK11195 challengers. *Eur. J. Nucl. Med. Mol. Imaging* **2008**, *35*, 2304–2319.
(18) Venneti, S.; Lopresti, B. J.; Wiley, C. A. The peripheral benzodiazepine receptor (translocator protein 18 kDa) in microglia: from pathology to imaging. *Prog. Neurobiol.* **2006**, *80*, 308–322.
(19) Petit-Taboué, M. C.; Baron, J. C.; Barré, L.; Travere, J. M.; Speckel, D.; Camsonne, R.; MacKenzie, E. T. Brain kinetics and specific binding of [$^{11}$C]PK11195 to $\omega_3$ sites in baboon. *Eur. J. Pharmacol.* **1991**, *200*, 347–351.
(20) Camsonne, R.; Moulin, M. A.; Crouzel, C.; Syrota, A.; Maziere, M.; Comar, D. $^{11}$C-labeling of PK 11195 and visualization of peripheral receptors of benzodiazepines by positron emission tomography. *J. Pharmacol.* **1986**, *17*, 383.
(21) Shah, F.; Hume, S. P.; Pike, V. W.; Ashworth, S.; McDermott, J. Synthesis of the enantiomers of [*N*-methyl-$^{11}$C]PK 11195 and comparison of their behaviours as radioligands for PK binding sites in rats. *Nucl. Med. Biol.* **1994**, *21*, 573–581.
(22) Imaizumi, M.; Briard, E.; Zoghbi, S. S.; Gourley, J. P.; Hong, J.; Fujimura, Y.; Pike, V. W.; Innis, R. B.; Fujita, M. Brain and whole-body imaging in nonhuman primates of [$^{11}$C]PBR28, a promising PET radioligand for peripheral benzodiazepine receptors. *NeuroImage* **2008**, *39*, 1289–1298.
(23) Briard, E.; Zoghbi, S. S.; Imaizumi, M.; Gourley, J. P.; Shetty, H. U.; Hong, J.; Cropley, V.; Fujita, M.; Innis, R. B.; Pike, V. W. Synthesis and evaluation in monkey of two sensitive $^{11}$C-labeled aryloxyanilide ligands for imaging brain peripheral benzodiazepine receptors in vivo. *J. Med. Chem.* **2008**, *51*, 17–30.
(24) Fujita, M.; Imaizumi, M.; Zoghbi, S. S.; Fujimura, Y.; Farris, A. G.; Suhara, T.; Hong, J.; Pike, V. W.; Innis, R. B. Kinetic analysis in healthy humans of a novel positron emission tomography radioligand to image the peripheral benzodiazepine receptor, a potential biomarker for inflammation. *NeuroImage* **2008**, *40*, 43–52.
(25) Kreisl, W. C; Fujita, M.; Fujimura, Y.; Kimura, N.; Jenko, K. J.; Kannan, P.; Hong, J.; Morse, C. L.; Zoghbi, S. S.; Gladding, R. L.; Jacobson, S.; Oh, U.; Pike, V. W.; Innis, R. B. Comparison of [$^{11}$C](*R*)-PK 11195 and [$^{11}$C]PBR28, two radioligands for translocator protein (18 kDa) in human and monkey: implications for positron emission tomographic imaging of this inflammation biomarker. *NeuroImage* **2010**, *49*, 2924–2932.
(26) Owen, D. R.; Howell, O. W.; Tang, S.-P.; Wells, L. A.; Bennacef, I.; Bergstrom, M.; Gunn, R. N.; Rabiner, E. A.; Wilkins, M. R.; Reynolds, R.; Matthews, P. M.; Parker, C. A. Two binding sites for [$^{3}$H]PBR28 in human brain: implications for TSPO PET imaging of neuroinflammation. *J. Cereb. Blood Flow Metab.* **2010**, *30*, 1608–1618.
(27) Primofiore, G.; Da Settimo, F.; Taliani, S.; Simorini, F.; Patrizi, M. P.; Novellino, E.; Greco, G.; Abignente, E.; Costa, B.; Chelli, B.; Martini, C. *N*,*N*-Dialkyl-2-phenylindol-3-ylglyoxylamides. A new class of potent and selective ligands at the peripheral benzodiazepine receptor. *J. Med. Chem.* **2004**, *47*, 1852–1855.
(28) Da Settimo, F.; Simorini, F.; Taliani, S.; La Motta, C.; Marini, A. M.; Salerno, S.; Bellandi, M.; Novellino, E.; Greco, G.; Cosimelli, B.; Da Pozzo, E.; Simola, N.; Morelli, M.; Martini, C. Anxiolytic-like effects of *N*,*N*-dialkyl-2-phenylindol-3-ylglyoxylamides by modulation of translocator protein promoting neurosteroid biosynthesis. *J. Med. Chem.* **2008**, *51*, 5798–806.
(29) Pike, V. W. Positron-emitting radioligands for studies in vivo—probes for human psychopharmacology. *J. Psychopharmacol.* **1993**, *7*, 139–158.
(30) Laruelle, M.; Slifstein, M.; Huang, Y. Relationships between radiotracer properties and image quality in molecular imaging of the brain with positron emission tomography. *Mol. Imaging Biol.* **2003**, *5*, 363–375.
(31) Waterhouse, R. N. Determination of lipophilicity and its use as a predictor of blood−brain barrier penetration of molecular imaging agents. *Mol. Imaging Biol.* **2003**, *5*, 376–389.
(32) Pike, V. W. PET Radiotracers: crossing the blood−brain barrier and surviving metabolism. *TIPs* **2009**, *30*, 431–440.
(33) Briard, E.; Zoghbi, S. S.; Siméon, F.; Imaizumi, M.; Gourley, J. P.; Shetty, H. U.; Lu, S.-Y.; Fujita, M.; Innis, R. B.; Pike, V. W. Single-step high-yield radiosynthesis and evaluation of a selective $^{18}$F-labeled ligand for imaging brain peripheral benzodiazepine receptors with PET. *J. Med. Chem.* **2009**, *52*, 688–699.
(34) Owen, D. R.; Gunn, R. N; Rabiner, E. A.; Bennacef, I.; Fujita, M.; Kreisl, W. C.; Innis, R. B.; Pike, V. W.; Reynolds, R.; Matthews, P. M.; Parker C. A. Mixed affinity binding in humans with 18 kDa translocator protein (TSPO) ligands. *J. Nucl. Med.* in press.
(35) Cheng, Y.; Prusoff, W. H. Relationship between constant ($K_i$) and the concentration of inhibitor which causes 50% inhibition ($IC_{50}$) of an enzymatic reaction. *Biochem. Pharmacol.* **1973**, *22*, 3099–3108.
(36) Braestrup, C.; Squires, R. F. Specific benzodiazepine receptors in rat brain characterized by high-affinity [$^{3}$H)]diazepam binding. *Proc. Natl. Acad. Sci. U.S.A.* **1977**, *74*, 3805–3809.
(37) Karobath, M; Sperk, G. Stimulation of benzodiazepine receptor binding by $\gamma$-aminobutyric acid. *Proc. Natl. Acad. Sci. U.S.A.* **1979**, *76*, 1004–1006.
(38) Costanzo, A.; Guerrini, G.; Ciciani, G.; Bruni, F.; Selleri, S.; Costa, B.; Martini, C.; Lucacchini, A.; Aiello, P. M.; Ipponi, A. Benzodiazepine receptor ligands. 4. Synthesis and pharmacological evaluation of 3-heteroaryl-8-chloropyrazolo[5,1-*c*][1,2,4] benzotriazine 5-oxides. *J. Med. Chem.* **1999**, *42*, 2218–2226.
(39) Christman, D. R.; Finn, R. D.; Karlström, K.; Wolf, A. P. The production of ultra high specific activity $^{11}$C-labeled hydrogen cyanide, carbon dioxide, carbon monoxide and methane via the $^{14}$N(p,$\alpha$)$^{11}$C reaction. *Int. J. Appl. Radiat. Isot.* **1975**, *26*, 435–442.
(40) Larsen, P.; Ulin, J.; Dahlström, K.; Jensen, M. Synthesis of [$^{11}$C]iodomethane by iodination of [$^{11}$C]methane. *Appl. Radiat. Isot.* **1997**, *48*, 153–157.
(41) Clark, J. D.; Baldwin, R. L.; Bayne, K. A.; Brown, M. J.; Gebhart, G. F.; Gonder, J. C.; Gwathmey, J. K.; Keeling, M. E.; Kohn, D. F.; Robb, J. W.; Smith, O. A.; Steggerda, J.-A. D.; VandeBer, J. L. *Guide for the Care and Use of Laboratory Animals*; National Academy Press: Washington DC, 1996.
(42) Gandelman, M. S.; Baldwin, R. M.; Zoghbi, S. S.; Zea-Ponce, Y.; Innis, R. B. Evaluation of ultrafiltration for the free-fraction determination of single photon emission computed tomography (SPECT) radiotracers: $\beta$-CIT, IBF, and iomazenil. *J. Pharm. Sci.* **1994**, *83*, 1014–1019.